Hybrid fiber Bragg grating sensor for vibration and temperature monitoring of a train bearing

Xiaofeng Wang (王小峰)[1,2], Yongxing Guo (郭永兴)[3,*], and Li Xiong (熊 丽)[4]

[1]*School of Communication, Shenzhen University, Shenzhen 518060, China*

[2]*School of Political Science and Public Management, Wuhan University, Wuhan 430072, China*

[3]*Key Laboratory of Metallurgical Equipment and Control Technology, Ministry of Education, Wuhan University of Science and Technology, Wuhan 430081, China*

[4]*Hubei Key Laboratory of Mechanical Transmission and Manufacturing Engineering, Wuhan University of Science and Technology, Wuhan 430081, China*

**Corresponding author: yongxing_guo@wust.edu.cn*

Received April 3, 2018; accepted May 14, 2018; posted online June 29, 2018

We report a fiber Bragg grating (FBG)-based sensor for the simultaneous measurement of a train bearing's vibration and temperature. A pre-stretched optical fiber with an FBG and a mass is designed for axial vibration sensing. Another multiplexed FBG is embedded in a selected copper-based alloy with a high thermal expansion to detect temperature. Experiments show that the sensor possesses a high resonant frequency of 970 Hz, an acceleration sensitivity of 27.28 pm/g, and a high temperature sensitivity of 35.165 pm/°C. A resonant excitation test is also carried out that demonstrates the robustness and reliability of the sensor.

OCIS codes: 060.3735, 060.2370, 280.4788.

doi: 10.3788/COL201816.070604.

Temperature rising of a bearing directly affects the bearing life, so the bearing temperature is currently one of the most important parameters in the monitoring system of a train[1]. The vibration signal of a bearing contains important fault information that is also significant for ensuring the safety of the train operation[2]. By the end of 2017, China's railway operating mileage had reached 127,000 km, including a high-speed railway of 25,000 km, however, the normal-speed railway had been still in the majority (over 80.3%). Unlike the seamless rails used in a high-speed railway, seams exist in the rails of a normal-speed railway. With several speeds increasing for the normal-speed railway, the problem of vibration shock of a train's bearings due to rail seams is becoming more and more prominent. Therefore, besides the traditional temperature monitoring, consideration of vibration monitoring is needed now, which requires new sensors for both temperature and vibration monitoring of the normal-speed train bearings.

As a particular class of optical fiber sensors, a fiber Bragg grating (FBG) has been proven to be very effective because of its inherent advantages, such as immunity to electromagnetic interference and optical power fluctuations, small profile, light weight, no zero temperature drift, and the fact that multiple FBGs can be arrayed along a single fiber[3–5]. During the past few decades, FBG sensors have been widely used in civil engineering[6], structural health monitoring[7], and robotics[8–10]. FBG-based vibration sensors/accelerometers mainly involve using a cantilever beam and its evolution types with an attached FBG to detect alternate strain brought by vibration deformation[11–13]. However, these cantilever-based structures have the deficiency that its resonant frequency and sensitivity severely restrict each other, which can not satisfy the actual demand that the bearing often vibrates with hundreds of hertz and a small acceleration. Several accelerometers with a high resonance frequency or sensitivity have been reported, such as using a polymer optical FBG[14], multi-flexible hinges[15], and a hexagonal lattice hollow cylinder[16], however, these designs suffered from high cost, complex structure and fabrication, or big bulk. Accelerometers with a spring-mass structure vibrate along the FBG axis and have many advantages such as compact size, low weight, and high frequency[17–19]. The axial vibration deformation directly transforms into the axial strain of the FBG and brings a wavelength shift, which can achieve a high resonance frequency and sensitivity. Through using the axial property to measure vibration, separately fixing the double-end of the FBG on the base, and arranging the mass between two diaphragms, accelerometers with a resonant frequency of 1240 Hz have been produced[20]. Zhu *et al.*[21] proposed a dual FBG accelerometer by using lantern-shaped metallic shells and achieved a resonant frequency of 1175 Hz and a sensitivity of 9.4 pm/g.

This Letter introduces our work on an FBG-based hybrid sensor for vibration and temperature monitoring of a train bearing. A single-mode optical fiber with an FBG and a mass has been pre-stretched and two ends have been fixed by glass solder to detect the axial vibration. Another FBG has been embedded in a selected copper-based alloy with a high thermal expansion to enhance the temperature sensitivity of the FBG and to serve as a temperature probe of the hybrid sensor. The mechanical structure design, sensing principle, and performance test have been presented in detail below.

Figure 1 shows the installation situation of a traditional temperature sensor on the train bearing. The sensor is

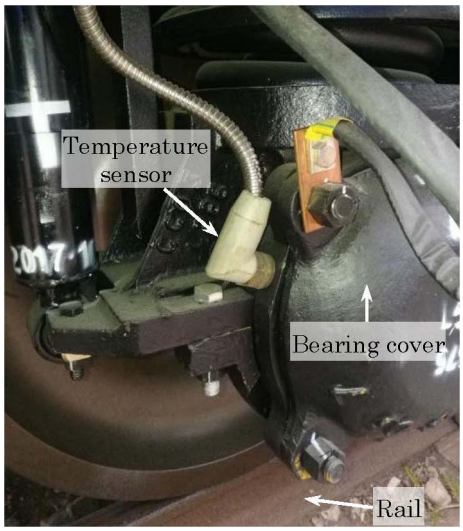

Fig. 1. Installation situation of a traditional temperature sensor.

installed through a screw hole in the bearing cover and the temperature probe at the top part of the sensor is guided to touch the outer ring of the bearing. Considering the existing installation standard, the schematic diagram of the proposed hybrid sensor is shown in Fig. 2.

The sensor mainly includes an optical fiber with two FBGs, a mass, a temperature probe, an end cover, and a shell with a mounting thread matched with the screw hole in the bearing cover. FBG2 is embedded and fixed in the micro hole of the temperature probe made of a copper-based alloy with a high thermal expansion to enhance the temperature measuring sensitivity of FBG2. The optical fiber passes through the mass and is fixed by glass solder. The mass is inserted into the shell with a transition fit, which permits free sliding along the axial direction and restricts radial movement. Then the fiber on the left side of FBG2 is fixed on a temperature probe by glass solder and the temperature probe is fixed in the shell. After an axial pre-tension, the fiber on the left side of the mass is also fixed on the end cover. Where the fiber is being fixed by glass solder it is bared without a polymer coating, and the temperature for the fixation of glass solder is about 130°C. The pre-stretching optical fiber is used as a spring element, and the FBG1 output undergoes a wavelength shift caused by the inertial force of the axial mass movement driven by the axial vibration. The corresponding theoretical derivation is presented as follows.

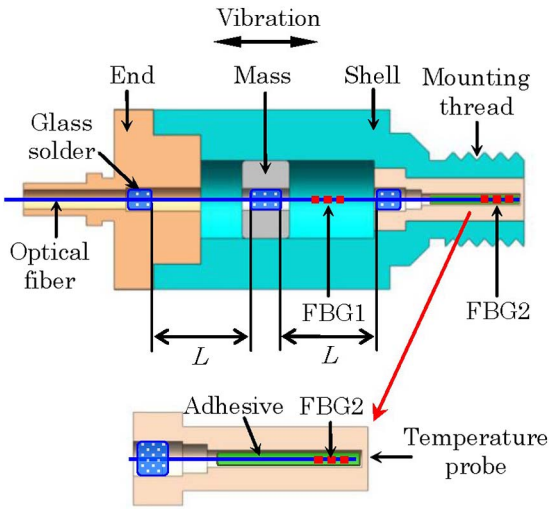

Fig. 2. Schematic diagram of the proposed FBG hybrid sensor.

The wavelength–strain relationship of FBG1 can be expressed as

$$\Delta\lambda = (1 - p_e) \cdot \varepsilon \cdot \lambda, \tag{1}$$

where $\Delta\lambda$ is the wavelength drift, p_e is the elasto-optical coefficient, ε is the axis strain, and λ is the initial wavelength of the FBG.

The relationship between strain and acceleration in the proposed vibration structure is

$$a = \frac{F}{m} = \frac{2ES}{m} \cdot \varepsilon, \tag{2}$$

where F is the vibration inertia force on the mass, S is the cross-sectional area of the optical fiber, m is the mass quality, and $E = (E_1 V_1 + E_2 V_2)/V$ is the Young's modulus of the composite composed of a cladding and coating layer for the optical fiber. E_1 and E_2 stand for the Young's modulus of the cladding and coating layer, respectively, whereas V_1 and V_2 stand for the volume of the cladding and coating layer, respectively. V is the volume of the optical fiber. By combining Eqs. (1) and (2), the relationship between acceleration and the FBG1 wavelength shift could be deduced as

$$\frac{\Delta\lambda}{\lambda} = \frac{m(1 - p_e)}{2ES} \cdot a. \tag{3}$$

From Eq. (2), the elastic coefficient k of the optical fiber could be presented as

$$F = 2ES \cdot \varepsilon = 2ES\frac{\Delta L}{L} = \left(\frac{2ES}{L}\right) \cdot \Delta L = k \cdot \Delta L,$$
$$k = \frac{2ES}{L}. \tag{4}$$

Here, as shown in Fig. 2, the optical fiber between the two fixed points on the temperature probe and the end cover is divided into two parts by the mass, and L represents the length of each segment. Therefore, the resonant frequency of the accelerometer is given by

$$f = \frac{1}{2\pi}\sqrt{\frac{k}{m}} = \frac{1}{2\pi}\sqrt{\frac{2ES}{mL}}. \tag{5}$$

Obviously, the E and S values of the optical fiber are constants, so the resonant frequency is determined by m and L. The parameters of the optical fiber are as follows: $E_1 = 73$ GPa, $E_2 = 2.55$ GPa, and the diameters of the

fiber cladding and coating layer are $d_1 = 0.125$ mm and $d_2 = 0.25$ mm.

Then, further analysis was carried out to investigate the relationship between the resonant frequency and the parameters of m and L. Considering a value of L from 10 to 21 mm with a step of 0.5 mm, and m from 1 to 6 g with a step of 0.5 g, the relation between length L, weight m, and the resonant frequency has been presented in Fig. 3. Considering that a bearing often vibrates with hundreds of hertz, the parameters have been chosen as $L = 15$ mm and $m = 4$ g, which corresponds to a theoretical resonant frequency of about 914.373 Hz. For temperature monitoring, FBG2 is embedded and fixed in the micro hole of the temperature probe, so the wavelength shift of FBG2 changes with the expansion and contraction of the copper-based alloy due to the temperature variation.

Two FBGs with a reflectivity of 90% and a bandwidth of 0.2 nm have been made by a femtosecond laser using phase mask technology and used to fabricate a sensor prototype. After an axial pre-tension of about 1.241 nm for FBG1, a sensor prototype with a central wavelength of 1546.94 nm for FBG1 and 1533.75 nm for FBG2 has been manufactured, as shown in Fig. 4. The diameter of the sensor prototype is $D = 23$ mm, the total height is 52 mm, and the weight is 86.4 g.

As shown in Fig. 5, a vibration test system has been established to measure the time and linearity response of the sensor. A homemade FBG interrogator (acquisition frequency: 8000 Hz, accuracy: 3 pm, resolution: 0.1 pm) is used to record the wavelength of the sensor. The

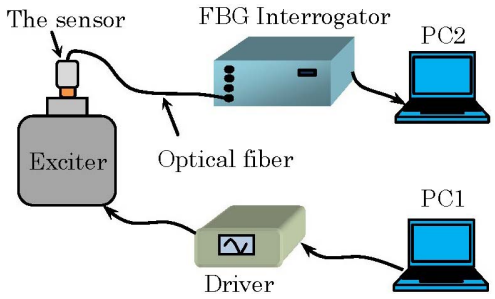

Fig. 5. Experimental setup of the vibration test.

amplitude–frequency characteristic of the sensor is investigated through excitation with a frequency band from 10 Hz to 1400 Hz, whereas the input acceleration is kept constant at g ($g = 10$ m/s^2). Figure 6 shows the amplitude–frequency response curve, which indicates that the resonant frequency is 970 Hz and is basically consistent with the theoretical resonant frequency of 914.373 Hz. The flat response region is up to 500 Hz, which meets the bearing vibration requirements. The time response capability is plotted in Fig. 7. Under an acceleration of $0.5g$, satisfactory response waveforms at the excitation frequencies of 50, 150, and 300 Hz are observed, which demonstrates an excellent dynamic measurement capability.

The linear response capability is investigated. During this test period, the vibration acceleration is raised from 5 m/s^2 to 60 m/s^2, whereas the vibration frequency is kept at 160 Hz. The test is repeated for three times.

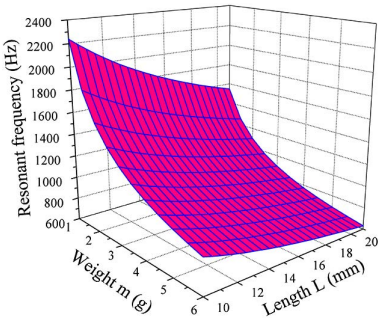

Fig. 3. Relation between length L, weight m, and the resonant frequency.

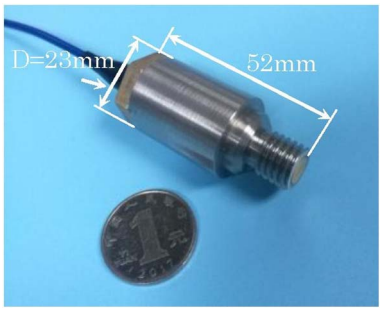

Fig. 4. Photo of the hybrid FBG sensor.

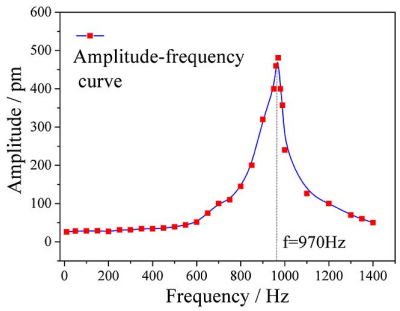

Fig. 6. Amplitude–frequency response curve.

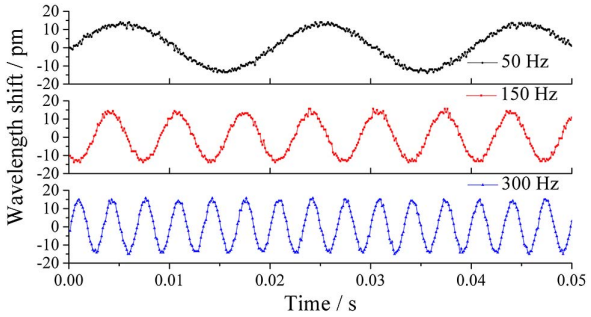

Fig. 7. Time response capability under different vibration frequencies.

The amplitude response and the fitting function of average values are shown in Fig. 8. The sensitivity of the sensor is observed to be 27.28 pm/g with a linearity of 0.9994, and the repeatability error is 5.02% for three independent tests. By considering the FBG interrogator measuring resolution of 3 pm, we can determine that the sensor can measure acceleration with the accuracy of $3/(27.28) = 0.11g$, which could satisfy the bearing vibration requirement.

As a one-dimensional sensor, anti-interference in the transverse (radial) direction is inescapable in real-world applications. An excitation test is carried out along the working (axial) direction and the transverse direction. During this test, the excitation frequency is kept at 100 Hz, and excitation accelerations are set at $2g$. Responses in the work and transverse directions are shown in Fig. 9, wavelength shifts of the transverse directions are all very small (about 8 pm), which demonstrates that the sensor has a good anti-interference and also indicates that the design of the transition fit between the mass and the shell restricts the interferential radial movement.

As the pre-stretching optical fiber is used as a spring element and will undergo frequent alternating strain, the reliability of the glass solder fixation and the maintenance of pre-tension are very important for long time service. It is well known that a vibration sensor should avoid being in the resonant environment because the sensor will be easily damaged by strong vibrations with huge amplitude. But here we just use the resonance to verify the robustness of the glass solder fixation and the pre-tension of the fiber. During this test, the excitation frequency is kept at 1000 Hz (close to the resonance frequency of 970 Hz),

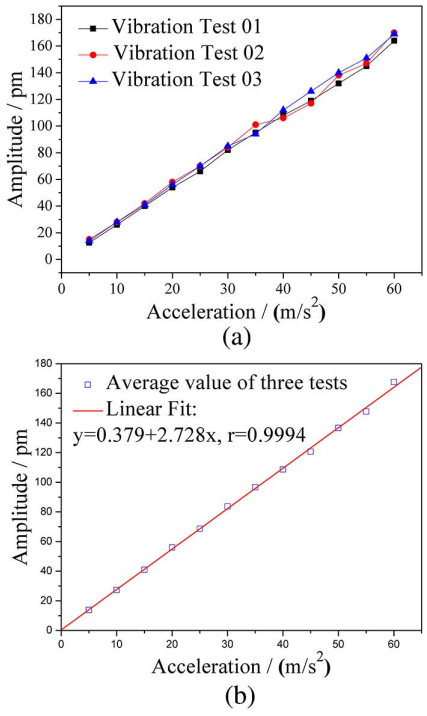

Fig. 8. Linear response test: (a) the three test results, and (b) the linear fitting of the average test data.

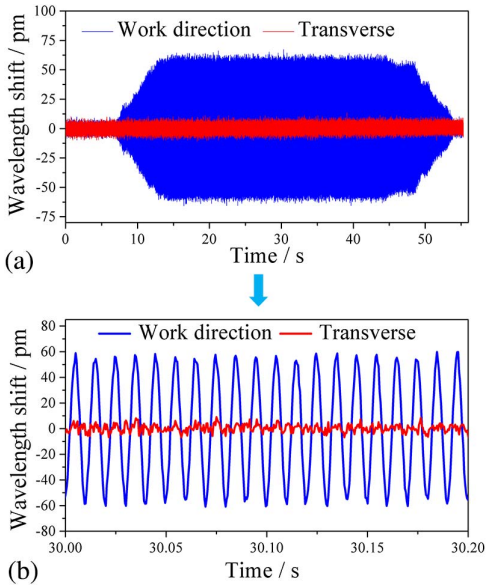

Fig. 9. (a) Wavelength shift responses in the work and transverse directions, and (b) an enlarged view of the local data.

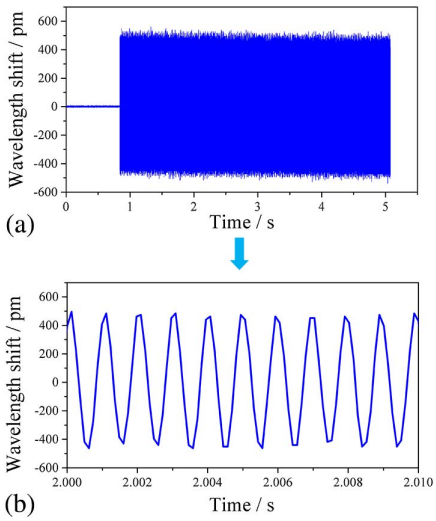

Fig. 10. (a) Part of the experimental data for the reliability test, and (b) an enlarged view of the local data.

and excitation accelerations are set at $2g$. Figure 10 shows part of the experimental data recorded, from which we can see that the resonance amplitude is as large as 0.5 nm. The pre-tension amount, resonant frequency, and sensitivity of the sensor have been investigated after the resonant excitation. Table 1 shows the changing situation of the above three key parameters at different excitation numbers. All three parameter values have no abnormal change, which demonstrates that the harsh resonant excitation does not degrade the sensor performance and thus demonstrates the robustness and reliability of the sensor.

Finally, the temperature measuring ability of FBG2 in the sensor is investigated. During the test, a thermostat (OTF-1200X, HEFEI KE JING Materials Technology Co., Ltd., China; accuracy: 1°C, resolution: 0.1°C) is used to change the surrounding temperature of the sensor.

Table 1. Changing Situation of the Above Three Key Parameters at Different Excitation Numbers

Excitation Time (s)	Corresponding cycle number	Pre-tension amount (nm)	Sensitivity (pm/g)	Resonant frequency (Hz)
0	0	1.241	27.28	970
1	10^3	1.247	28.13	975.5
10	10^4	1.24	28.09	971
100	10^5	1.243	27.56	965
1000	10^6	1.245	28.33	961

The temperature is changed from room temperature (18°C) to 20°C, then to 100°C with a sampling interval of 10°C. The wavelength shift at each temperature point is recorded. As shown in Fig. 11(a), a linear fit has been carried out for the wavelength shift values at the temperature test points. From the linear fitted curve, the temperature sensitivity is observed to be 35.165 pm/°C with a linearity of 0.9978, and the sensitivity is about 3.06 times that of the theoretical sensitivity (11.5 pm/°C) of a bare FBG with a center wavelength at 1533 nm, which demonstrates the effectivity of the enhanced sensitivity design. In addition, the test data is also polynomial fitted, as shown in Fig. 11(b), which shows a better correlation coefficient of 0.9991. The two measurement functions can be chosen according to actual application requirements.

This work has described the design, implementation, and test of a hybrid FBG vibration and temperature sensor for a train bearing. The use of an axial elastic structure promises a high resonant frequency of 970 Hz and a sensitivity of 27.28 pm/g. The resonant frequency and sensitivity of this sensor can be adjusted freely by modifying the working length of the suspended optical fiber and changing the quality of the mass. In addition, the friction between the mass and the shell, which has an influence on the sensor's parameters, could be reduced by using a lubricant, precision machining, and assembly. An enhanced sensitivity design has been implemented for temperature measuring by using a copper-based alloy with high thermal expansion, and a high temperature sensitivity of 35.165 pm/°C is obtained. Both vibration and temperature detection performances satisfy the train bearing requirement.

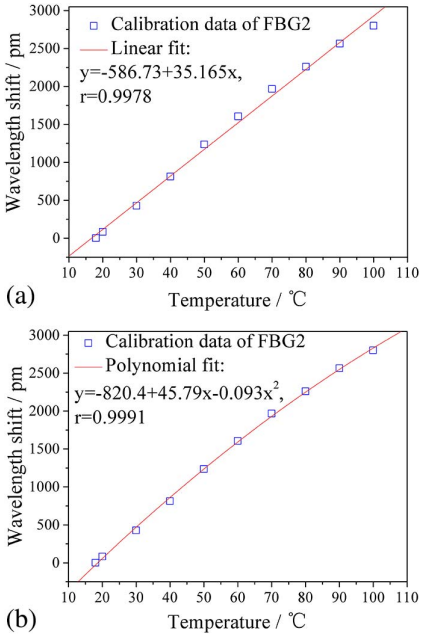

Fig. 11. Temperature test results: (a) the linear fitting result, and (b) the polynomial fitting result.

Compared to the traditional electrical sensor, the proposed sensor can significantly improve the performance of electromagnetic anti-interference in an electrified train. However, FBG-based sensors require a high-cost investment in the associated interrogator for the demodulation of the optical signal because the development of the FBG is fairly recent, and the state of its sensing technology is not completely mature. The sensing principle, manufacturing craft, and especially signal detecting technology/instrument are constantly being researched and developed. More testing work will be investigated in the train operating environment in the future to promote the performance of the sensor to the product level.

This work was supported in part by the National Natural Science Foundation of China (Nos. 51605348 and 51605344), in part by the Natural Science Foundation of the Hubei Province (No. 2016CFB116), and in part by the Open Research Fund of the Hubei Digital Manufacturing Key Laboratory (No. SZ1801).

References

1. W. Tang, M. Wang, G. Chen, Y. Sun, and L. Xu, J. China Railw. Soc. **38**, 50 (2016).
2. J. Ding, Measurement **117**, 108 (2018).
3. L. Xiong, D. S. Zhang, and L. T. Li, Chin. Opt. Lett. **12**, 120605 (2014).
4. Y. Pan, J. Jiang, W. Lu, H. Yang, K. Liu, S. Wang, H. Wang, and T. Liu, Chin. Opt. Lett. **15**, 070605 (2017).
5. L. Wang, M. Wan, and Z. Shen, Photon. Res. **5**, 219 (2017).
6. Y. Guo, D. Zhang, J. Fu, S. Liu, S. Zhang, and F. Zhu, Sens. Rev. **35**, 348 (2015).
7. Y. Guo, J. Kong, H. Liu, D. Hu, and L. Qin, IEEE Sens. J. **16**, 8456 (2016).

8. Y. Guo, J. Kong, H. Liu, H. Xiong, G. Li, and L. Qin, Sens. Actuators A **249**, 141 (2016).
9. L. Xiong, G. Jiang, Y. Guo, and H. Liu, IEEE Sens. J. **18**, 3632 (2018).
10. Z. Liu and H. Tam, Chin. Opt. Lett. **14**, 120007 (2016).
11. N. Basumallick, I. Chatterjee, P. Biswas, K. Dasgupta, and S. Bandyopadhyay, Sens. Actuators A **173**, 108 (2012).
12. N. Basumallick, P. Biswas, K. Dasgupta, and S. Bandyopadhyay, Sens. Actuators A **194**, 31 (2013)
13. M. M. Khana, N. Panwar, and R. Dhawan, Sens. Actuators A **205**, 79 (2014).
14. A. Stefani, S. Andresen, W. Yuan, N. Rasmussen, and O. Bang, IEEE Photon. Technol. Lett. **24**, 763 (2012).
15. L. Qiu, L. Liang, D. Li, and G. Xu, Opt. Fiber Technol. **38**, 142 (2017).
16. N. Gutiérrez, P. Galvín, and F. Lasagni, Measurement **117**, 295 (2018).
17. T. Li, C. Shi, Y. Tan, R. Li, Z. Zhou, and H. Ren, IEEE Sens. J. **17**, 1021 (2017).
18. T. Li, Y. Tan, and Z. Zhou, Sens. Actuators A **259**, 85 (2017).
19. Y. Guo, D. Zhang, Z. Zhou, L. Xiong, and X. Deng, Chin. Opt. Lett. **11**, 070604 (2013).
20. Q. Liu, X. Qiao, Z. Jia, H. Fu, H. Gao, and D. Yu, IEEE Sens. J. **14**, 1499 (2014).
21. J. Zhu, J. Wang, P. Gan, Z. Hu, and Y. Hu, IEEE Sens. J. **17**, 5130 (2017).